

SUPPLEMENTARY INFORMATION

Polymersomes decorated with SARS-CoV-2 spike protein receptor binding domain elicit robust humoral and cellular immunity

Lisa R. Volpatti^{1*}, Rachel P. Wallace^{1*}, Shijie Cao^{1*}, Michal M. Raczky^{1*}, Ruyi Wang^{1*}, Laura T. Gray¹, Aaron T. Alpar¹, Priscilla S. Briquez¹, Nikolaos Mitrousis¹, Tiffany M. Marchell², Maria Stella Sasso¹, Mindy Nguyen¹, Aslan Mansurov¹, Erica Budina¹, Ani Solanki³, Elyse A. Watkins¹, Mathew R. Schnorenberg¹, Andrew C. Tremain², Joseph W. Reda¹, Vlad Nicolaescu⁴, Kevin Furlong⁴, Steve Dvorkin⁴, Shann S. Yu¹, Balaji Manicassamy⁵, James L. LaBelle⁶, Matthew V. Tirrell^{1,7}, Glenn Randall⁴, Marcin Kwissa¹, Melody A. Swartz^{1,2,8,9+}, Jeffrey A. Hubbell^{1,2,9+}

*These authors contributed equally to this work

¹Pritzker School of Molecular Engineering, University of Chicago, Chicago, IL 60637, United States

²Committee on Immunology, University of Chicago, Chicago, IL 60637, United States

³Animal Resources Center, University of Chicago, Chicago, IL 60637, United States

⁴Department of Microbiology, Howard T. Ricketts Laboratory, University of Chicago, Chicago, IL 60637, United States

⁵Department of Microbiology and Immunology, University of Iowa, Iowa City, IA 52242, United States

⁶Department of Pediatrics, University of Chicago Comer Children's Hospital, Chicago, IL 60637, United States

⁷Materials Science Division, Argonne National Laboratory, Lemont, IL 60439, United States

⁸Ben May Department of Cancer Research, University of Chicago, Chicago, IL 60637, United States

⁹Committee on Cancer Biology, University of Chicago, Chicago, IL 60637, United States

+Correspondence to melodyswartz@uchicago.edu, jhubbell@uchicago.edu

Table of Contents

Methods

Figure S1. Synthesis and characterization of N₃-PEG-PPS.

Figure S2. Synthesis and characterization of RBD-linker.

Figure S3. Synthesis and characterization of PEG-PPS.

Figure S4. Additional cryoEM images of PS.

Figure S5. PS stability by SDS PAGE after > 180 d at 4 °C.

Figure S6. RBD binding to HEK-hACE2 and HEK-293 cells.

Figure S7. MPLA PS as a TLR4 agonist.

Figure S8. *In vitro* activity of MPLA PS.

Figure S9. ELISA absorbance vs. dilution curves.

Figure S10. Presence of IgA antibodies.

Figure S11. Accumulation of RBD_{surf} in injection site draining lymph nodes.

Figure S12. IgG antibody and viral neutralization titers.

Figure S13. Representative peptide array images.

Figure S14. Analysis of plasma by mice vaccinated with RBD_{surf} + RBD_{encap} + MPLA PS and RBD_{free} + MPLA_{free}.

Figure S15. Representative T follicular helper cell gating strategy.

Figure S16. Representative B cell gating strategy.

Figure S17. Total and naïve B cells in vaccinated mice 1 week post-boost.

Figure S18. Representative RBD protein tetramer staining.

Figure S19. RBD-specific cells in vaccinated mice 1 week post-boost.

Figure S20. Representative intracellular cytokine gating strategy.

Figure S21. Th2-type cytokines secreted upon *ex vivo* stimulation with RBD.

Table S1. Summary of loading capacities of PS.

Table S2. Probes and antibodies for T_{fh} cell panel.

Table S3. Probes and antibodies for RBD-specific B cell panel.

Table S4. Probes and antibodies for restimulation panel.

References

Methods

No unexpected or unusually high safety hazards were encountered conducting this work.

RBD production and purification

For production of the Spike protein RBD (Spike₃₁₉₋₅₄₁; GenBank: MN908947.3), we obtained expression plasmids on pCAGGS backbone containing mammalian codon-optimized sequences for this gene from Florian Krammer's laboratory (Icahn School of Medicine at Mount Sinai, New York, NY)¹. Suspension-adapted HEK-293F cells were maintained in serum-free Free Style 293 Expression Medium (Gibco). On the day of transfection, cells were inoculated at a concentration of 1×10^6 cells mL⁻¹. Plasmid DNA (1 mg mL⁻¹) was mixed with linear 25 kDa polyethylenimine (2 mg mL⁻¹; Polysciences) and co-transfected in OptiPRO SFM Medium (4% final concentration; Gibco). Flasks were cultured in an orbital shaking incubator (135 rpm, 37 °C, 5% CO₂) for 7 days. Culture medium was then collected by centrifugation, filtered, and loaded into a HisTrap HP 5 mL column (GE Healthcare) using an ÄKTA Pure 25 (GE Healthcare). After washing the column with wash buffer (20 mM NaH₂PO₄ and 0.5 M NaCl, pH 8.0), protein was eluted using a gradient of 500 mM imidazole in wash buffer. The protein was further purified by size-exclusion chromatography using a HiLoad Superdex 200PG column (GE Healthcare) with PBS as an eluent. Dimers of RBD were reduced by the addition of dithiothreitol (1 mM) which was subsequently dialyzed against PBS. All purification steps were carried out at 4 °C. The expressed proteins were verified to be >90% pure through SDS-PAGE. The purified proteins were tested for endotoxin using a HEK-Blue TLR4 reporter cell line (InvivoGen), and the endotoxin levels were confirmed to be below 0.01 EU mL⁻¹. Protein concentration was determined by absorbance at 280 nm using a NanoDrop spectrophotometer (Thermo Scientific). Proteins were stored at a concentration of 4 mg mL⁻¹ at -80 °C until use.

Chemical Synthesis and Characterization

N₃-PEG-PPS. N₃-PEG-PPS was synthesized by first dissolving N₃-PEG₂₄-SH (1 eq, MW ~1000 g mol⁻¹; Nanosoft Polymers) in degassed, anhydrous THF and deprotonating the thiol group by addition of sodium methoxide (NaOMe; 1.1 eq) under nitrogen gas. Propylene sulfide (40 eq) was added by syringe, and the reaction proceeded until completion at the desirable degree of polymerization of PPS, as determined by ¹H NMR. The polymer was precipitated multiple times in ice cold methanol to obtain the final product, N₃-PEG₂₄-PPS₄₀, characterized by ¹H NMR (400 MHz Bruker DRX spectrometer equipped with a BBO probe, using Topspin 1.3) and gel permeation chromatography (GPC; Tosoh EcoSEC size exclusion chromatography system with a Tosoh SuperAW3000 column). ¹H-NMR (400 MHz, CDCl₃) of N₃-PEG-PPS, δ 1.37 (s, PPS, 3H), 2.63 (m, PPS, 1H), 2.91 (m, PPS, 2H), 3.39 (t, -CH₂-N₃, 2H), 3.65 (m, PEG).

PEG-PPS. PEG-PPS was synthesized as previously described². Briefly, benzyl mercaptan (1 eq) in degassed, anhydrous THF (20 mM) was deprotonated with NaOMe (1.1 eq). Under nitrogen protection, propylene sulfide (39 eq) was rapidly added by syringe, and the reaction proceeded until completion at the desirable degree of polymerization of PPS, as determined by ¹H NMR. Subsequently, mPEG₁₇-mesylate (synthesized in-house as previously described¹) was added, and the mixture was allowed to react overnight. The polymer was precipitated multiple times in ice cold methanol to obtain the final product, PEG₁₇-PPS₃₀, characterized by ¹H NMR and GPC.

$^1\text{H-NMR}$ (400 MHz, CDCl_3) of mPEG-PPS, δ 1.37 (s, PPS, 3H), 2.63 (m, PPS, 1H), 2.91 (m, PPS, 2H), 3.38 (m, $-\text{OCH}_3$, 3H), 3.65 (m, PEG), 7.32 (m, benzyl, 4H).

PS formulation

Empty PS. Empty PEG-PPS polymersomes were formulated by thin film rehydration as previously described². In brief, 20 mg of polymer was dissolved in 750 μL dichloromethane (DCM), and DCM was removed by vacuum desiccation overnight. 1 mL of PBS was then added to the vial, which was rotated at room temperature (RT) for 24 h to allow complete dispersal of the polymer. The solution was then sequentially extruded through 0.8, 0.4, 0.2, and 0.1 μm pore membranes (Whatman).

RBD_{encap}. To formulate RBD-encapsulated PS, 250 μL of PBS containing 4 mg mL^{-1} RBD was added to the polymer thin film for rehydration, and the solution was rotated at 4 $^\circ\text{C}$ for 72 h before extrusion as above. After extrusion, RBD-encapsulated polymersomes were passed through a sepharose size exclusion chromatography (SEC) column to remove unencapsulated free RBD. The RBD content was quantified by SDS-PAGE using mini-protein TGX stain-free precast gels (Bio-Rad). Gels were imaged on a ChemiDoc XRS+ Gel Documentation System (Bio-Rad) and analyzed using ImageJ.

RBD_{surf}. RBD-surface-conjugated PS were synthesized by first formulating empty PS as above consisting of 25% N_3 -PEG-PPS to provide an excess of azide groups for conjugation. RBD was conjugated to a *sulfo* DBCO-Maleimide linker (Click Chemistry Tools) at the molar ratio of 1:5 (RBD:linker) and reacted for 2.5 h. Unconjugated linker was removed by Zeba spin desalting columns (7K MWCO; Thermo Scientific). The resulting RBD-linker was analyzed by MALDI-TOF MS using an α -cyano-4-hydroxycinnamic acid matrix (Sigma-Aldrich) and a Bruker ultrafleXtreme MALDI TOF/TOF instrument. RBD-linker (4 wt% of polymersome) was then incubated with empty N_3 -PEG-PPS polymersomes overnight at RT. The percentage of RBD-linker was optimized to achieve similar RBD loading as in RBD_{encap} to directly compare the two formulations. RBD-surface-conjugated PS were then passed through SEC to remove unconjugated RBD-linker. The conjugation was monitored by SDS-PAGE, and the final RBD content was quantified by the CBQCA Protein Quantitation Kit (Invitrogen). Based on nanoparticle concentration measured by NanoSight (5×10^{12} particles mL^{-1}), polymer concentration quantified by GPC (~ 5 mg mL^{-1}), and RBD loading (1.57 wt%), we calculated that approximately 380 copies of RBD are conjugated to a single polymersome. The average number of Spike protein trimers on a single SARS-CoV-2 virion can vary from 10-127³⁻⁵. Since our polymersomes are slightly larger than a virus particle, the surface density may be comparable or greater than that of SARS-CoV-2 virions.

Fluorescently labeled PS were prepared by conjugating AlexaFluor-647 alkyne dye (Invitrogen) to PS containing 25% N_3 -PEG-PPS. The dye was mixed with PS at a molar ratio of 1:20 (dye: N_3 -PEG-PPS), and the solution was stirred overnight at RT. Labeled PS were then passed through SEC to remove unconjugated dye. To make fluorescent RBD_{surf}, labeled PS were prepared as above and conjugated with RBD as described, followed by SEC purification. Final RBD content was quantified by the CBQCA Protein Quantitation Kit.

MPLA PS. MPLA PS were fabricated by flash nanoprecipitation using a 3D printed impingement jets mixer^{6,7}. 20 mg PEG-PPS and 2 mg MPLA (PHAD®; Avanti Polar Lipids) were dissolved in 500 μL tetrahydrofuran (THF) and loaded into a 1 mL plastic disposable syringe. 500 μL PBS was loaded into a second syringe, and the two solutions were impinged against one another slowly

within the mixer by hand. The impinged solution was immediately vortexed to form a homogenous PS solution which was then extruded and purified by SEC as described above. MPLA loading was quantified using a liquid chromatography-tandem mass spectrometry (LC-MS/MS) method as previously described⁸ using PHAD®-504 (Avanti Polar Lipids) as an internal standard on an Agilent 6460 Triple Quad MS-MS with 1290 UHPLC.

PS characterization

The size and polydispersity index (PDI) of all the PS formulations were measured by dynamic light scattering (DLS) using a Zetasizer Nano ZS90 (Malvern Instruments). Cryogenic electron microscopy (cryoEM) images were obtained on a FEI Talos 200kV cryoEM dedicated electron microscope.

MPLA PS *in vitro* activity

To determine TLR4 activation, HEK-Blue TLR4 cells (Invivogen) were incubated with increasing concentrations of MPLA PS for 24 h 37 °C in a 5% CO₂ incubator. NF-κB-induced SEAP activity was detected using QUANTI-Blue (Invivogen) and by reading the OD at 650 nm. For dendritic cell activation experiments, BMDCs were prepared from C57BL/6 mice (Jackson Laboratory) as previously described⁹. After 9 days of culture, cells were seeded at 2×10⁵ cells/well in round-bottom 96-well plates (Fisher Scientific) in IMDM with 10% FBS and 2% penicillin/streptomycin (Life Technologies). Cells were treated with varying concentrations of MPLA PS or free MPLA and incubated for 24 h at 37 °C in a 5% CO₂ incubator. After 24 h, the supernatant was collected, and cytokine concentration was measured using a multiplexed mouse Th cytokine panel (BioLegend) according to the manufacturer's instructions.

RBD_{surf} *in vitro* activity

For the cell-based hACE2-binding assay, human embryonic kidney (HEK)-293T cells overexpressing human ACE-2 (HEK-hACE2) were obtained from BEI Resources (NIH NIAID). Fluorescently labeled empty PS, RBD_{surf}, or RBD_{free} was incubated at varying concentrations with 5×10⁴ HEK-hACE2 cells at 4 °C for 20 min. Cells were then washed three times in PBS with 2% FBS. Binding of RBD to hACE-2 on the cell surface was assessed via the mean fluorescent intensity measured by flow cytometry using a BD LSRFortessa (BD Biosciences).

Production of RBD protein tetramers

RBD protein expressed with AviTag was purchased from GenScript. Site-specific biotinylation of the AviTag was performed using BirA Biotin-Protein Ligase Reaction kit (Avidity). Next, unconjugated biotin was removed using Zeba spin desalting columns, 7K MWCO (Thermo Scientific). The quantification of reacted biotin was performed using the Pierce Biotin Quantification Kit (Thermo Scientific). Biotinylated RBD was incubated with either streptavidin-conjugated PE or streptavidin-conjugated APC fluorophores (Biolegend) for 20 min on ice at a molar ratio of 4:1 of biotin to streptavidin. Streptavidin-conjugated FITC (BioLegend) was reacted with excess free biotin to form a non-RBD-specific streptavidin probe as a control. Tetramer

formation was confirmed using SDS-PAGE gel. Cells were stained for flow cytometry with all three streptavidin probes at the same time as other fluorescent surface markers at a volumetric ratio of 1:100 for RBD-streptavidin-PE and 1:200 for RBD-streptavidin-APC and biotin-streptavidin-FITC.

Mouse vaccination experiments

All experiments were performed in accordance with the Institutional Animal Care and Use Committee at the University of Chicago. Female 8-week-old C57BL/6 mice (Jackson Laboratory) were randomly assigned to cohorts of $n = 5$ and vaccinated with 10 μg of antigen and 5 μg of adjuvant s.c. in the hock (either 2 or 4 hocks) and boosted on day 21. On day 7, 14, 20, and 28 post vaccination, 100 μL of blood was collected in EDTA-K2-coated tubes (Milian), and plasma was separated by centrifugation and stored at $-80\text{ }^{\circ}\text{C}$ until use. On day 28 after initial vaccination, mice were sacrificed, and the spleen and injection site draining lymph nodes (brachial, axillary, popliteal, and inguinal) were collected.

Single-cell suspensions of the lymph node were prepared by digestion in collagenase D for 45 min at $37\text{ }^{\circ}\text{C}$. Splenocytes and lymph node cells were filtered through 70 μm cell strainers. Splenocytes were then incubated in ACK lysis buffer to remove red blood cells. Lymph node cells were stained for T_{fh} cells and RBD-specific B cells using fluorescent probes listed in Tables S1 and S2, respectively. Samples were acquired on a BD LSR-Fortessa (BD) and analyzed using FlowJo software. Representative gating strategies used to identify T_{fh} cells and RBD-specific B cells are shown in Figures S15 and S16, respectively.

To assess antigen-specific cytokine production by T cells, 1×10^6 lymph node cells were incubated with pools of 15-mer peptides overlapping by 10 amino acids covering the N-terminus of SARS-CoV-2 Spike protein up to the furin cleavage site (S1 pool; PepMix SARS-CoV-2 Spike Glycoprotein, JPT) for 6 h at $37\text{ }^{\circ}\text{C}$ with 5% CO_2 . Monensin (GolgiStop, BD) was added after 2 h of incubation to inhibit cytokine secretion. Cells were stained for surface markers using fluorescent probes. Cells were subsequently fixed and permeabilized using BD Cytotfix/Cytoperm, and intracellular cytokines were stained using fluorescent probes listed in Table S3. Samples were acquired on a BD LSR-Fortessa (BD) and analyzed using FlowJo software. A representative gating strategy used to identify the cell populations is shown in Figure S20. To assess antigen-specific cytokine secretion, lymph node cells were plated at 5×10^5 cells/well and incubated with 100 μg RBD for 3 d at $37\text{ }^{\circ}\text{C}$ with 5% CO_2 . After 3 d, the supernatant was analyzed for cytokine concentration via a multiplexed mouse Th cytokine panel (BioLegend) according to the manufacturer's instructions. Samples were acquired on an Attune NxT flow cytometer (ThermoFisher) and analyzed with LEGENDplex v8.0 software.

For long-term experiments, mice were bled on days 2, 7, and 14 and then every 2 weeks for 14 subsequent weeks. Mice treated with saline or RBD_{surf} were injected 19 weeks post-boost with AlexaFluor-647 labeled RBD_{surf} adjuvanted with MPLA PS. 24 h later, the popliteal and brachial draining LNs were collected, and the whole-organ fluorescence was measured using an IVIS Spectrum In Vivo Imaging System (Perkin Elmer). Images were processed and analyzed by Living Image 4.5.5 (Perkin Elmer).

RBD-binding ELISA

Plasma was assessed for anti-RBD IgG and IgA by ELISA. 96-well ELISA plates (Costar high-bind flat-bottom plates, Corning) were coated with $10 \mu\text{g mL}^{-1}$ RBD in carbonate buffer (50 mM sodium carbonate/sodium bicarbonate, pH 9.6) overnight at 4 °C. The following day, plates were washed three times in PBS with 0.05% Tween 20 (PBS-T) and then blocked with 1x casein (Sigma) for 2 h at RT. Following blocking, wells were washed three times with PBS-T and further incubated with six 10-fold dilutions of plasma in 1x casein for 2 h at RT. Wells were then washed five times with PBS-T and incubated for an additional 1 h at RT with horseradish peroxidase (HRP)-conjugated antibodies against mouse IgG, IgG1, IgG2b, IgG2c, IgG3, or IgA (Southern Biotech). After five washes with PBS-T, bound RBD-specific Ig was detected with tetramethylbenzidine (TMB) substrate. Stop solution (3% H_2SO_4 + 1% HCl) was added after 18 min of TMB incubation at RT, and the OD was measured at 450 and 570 nm on an Epoch Microplate Spectrophotometer (BioTek). Background signal at 570 nm was subtracted from the OD at 450 nm. Fold-change over the average of blank wells was then calculated and log-transformed. The area under the curve (AUC) of log-transformed fold change versus log-transformed dilution was then calculated.

RBD-binding IgG ELISpot assay

ELISpot plates (Millipore IP Filter plate) were coated with $20 \mu\text{g mL}^{-1}$ RBD in sterile PBS overnight at 4 °C. Plates were then blocked using ELISpot Media (RPMI 1640, 1% glutamine, 10% fetal bovine serum, 1% penicillin-streptomycin) for 2 h at 37 °C. Splenocytes from vaccinated mice were seeded in triplicate at a starting concentration of 6.75×10^5 cell/well and diluted seven times in 3-fold serial dilutions. Plates were incubated for 18 h at 37 °C and 5% CO_2 after which the cells were washed five times in PBS. Wells were incubated with 100 μL IgG-biotin HU adsorbed (Southern Biotech) for 2 h at RT. Next, plates were washed four times in PBS followed by the addition of 100 μL HRP-conjugated streptavidin/well for 1 h at RT. Plates were washed again and incubated with 100 μL TMB/well for 5 minutes until distinct spots emerged. Finally, plates were then washed three times with distilled water and left to dry completely in a laminar flow hood. A CTL ImmunoSpot Analyzer was used to image plates, count spots, and perform quality control.

SARS-CoV-2 virus neutralization assay

SARS-CoV-2 viruses (400 plaque forming units; strain nCov/Washington/1/2020, provided by the National Biocontainment Laboratory, Galveston TX, USA) were incubated with 4-fold serial dilutions of heat-inactivated plasma from vaccinated or control mice for 1 h at 37 °C in DMEM with 2% fetal bovine serum, 1% penicillin-streptomycin, and non-essential amino acids (10 mM, glycine, L-alanine, L-asparagine, L-aspartic acid, L-glutamic acid, L-proline, L-serine; Gibco). The pre-incubated viruses were then applied to Vero E6 cell monolayers, and the cells were maintained until > 90% cell death for the negative control (4-5 d). Cells were then washed with PBS, fixed with 10% formalin, stained with crystal violet, and quantified with a Tecan infinite m200 microplate reader (excitation/emission 592 nm/636 nm). Virus neutralization titer was quantified as the dilution that inhibits 50% of SARS-CoV-2 induced cell death (EC50). To determine the EC50, data were fit using a least squares variable slope four-parameter model. To ensure realistic EC50 values, we considered a dilution (1/X) of $X = 10^{-1}$ to be 100% neutralizing and a dilution of $X = 10^8$ to be 0% neutralizing and constrained $\text{EC}_{50} > 0$. Plasma from convalescent human

COVID-19 patients were provided by Ali Ellebedy (Washington University School of Medicine, St. Louis, MO; Catalog # NR-53661, NR-53662, NR-53663, NR-53664, and NR-53665).

Peptide array analysis

Antibody specificity to linear epitopes of the spike protein was analyzed using a CelluSpots Covid19_hullB Peptide Array (Intavis Peptide Services, Tubingen, Germany) according to the manufacturer's protocol. The array comprises 254 peptides spanning the full-length sequence of the Spike protein (NCBI GenBank accession # QHD43416.1), with each 15-mer peptide offset from the previous one by 5 amino acids. Briefly, peptide arrays were blocked in 1x casein solution at 4 °C overnight. Arrays were then incubated with pooled serum diluted 1:200 in 1x casein for 6 h at RT on an orbital shaker (60 rpm). After 6 h, arrays were washed four times with PBS-T and incubated for an additional 2 h at RT, 60 rpm with goat anti-mouse IgG conjugated to HRP (Southern Biotech) diluted 1:5000 in 1x casein. Arrays were washed another four times with PBS-T. Spots were detected with Clarity Western ECL Substrate (Bio-Rad), and chemiluminescence was measured using a ChemiDoc XRS+ Gel Documentation System (Bio-Rad). Spots were analyzed using Spotfinder software (version v3.2.1).

Software packages and statistical analysis

Statistical analysis was performed using GraphPad Prism 9 (GraphPad). Data were analyzed using one-way ANOVA with Dunn's or Tukey's post-hoc correction for multiple hypothesis testing unless otherwise stated. All flow cytometry data were analyzed using FlowJo_v10.7.2 software (FlowJo LLC, BD Biosciences). The TOC image, and Figures 1 and 2 were created using BioRender (<https://biorender.com>) as part of an Academic License through the Chicago Immunoengineering Innovation Center.

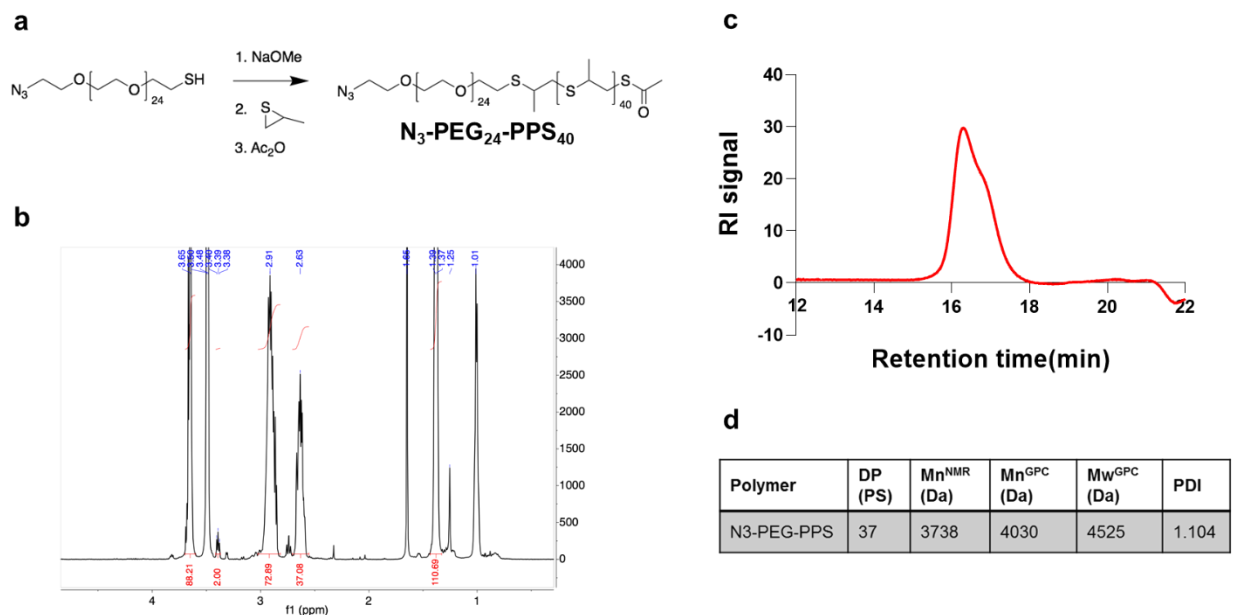


Figure S1 | Synthesis and characterization of N₃-PEG-PPS. **a**, Synthetic route, **b**, ¹H NMR spectrum, **c**, gel permeation chromatography (GPC) trace, and **d**, summary of physicochemical properties of N₃-PEG-PPS.

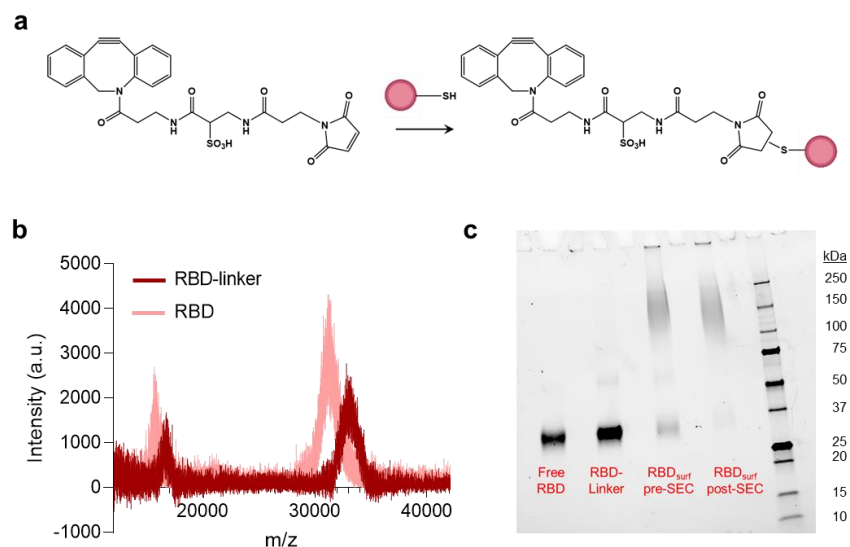


Figure S2 | Synthesis and characterization of RBD-linker. **a**, Synthetic route, **b**, MALDI of RBD-linker and free RBD, **c**, SDS PAGE of free RBD, RBD-linker, RBD_{surf} before size exclusion chromatography (SEC), and purified RBD_{surf} post-SEC.

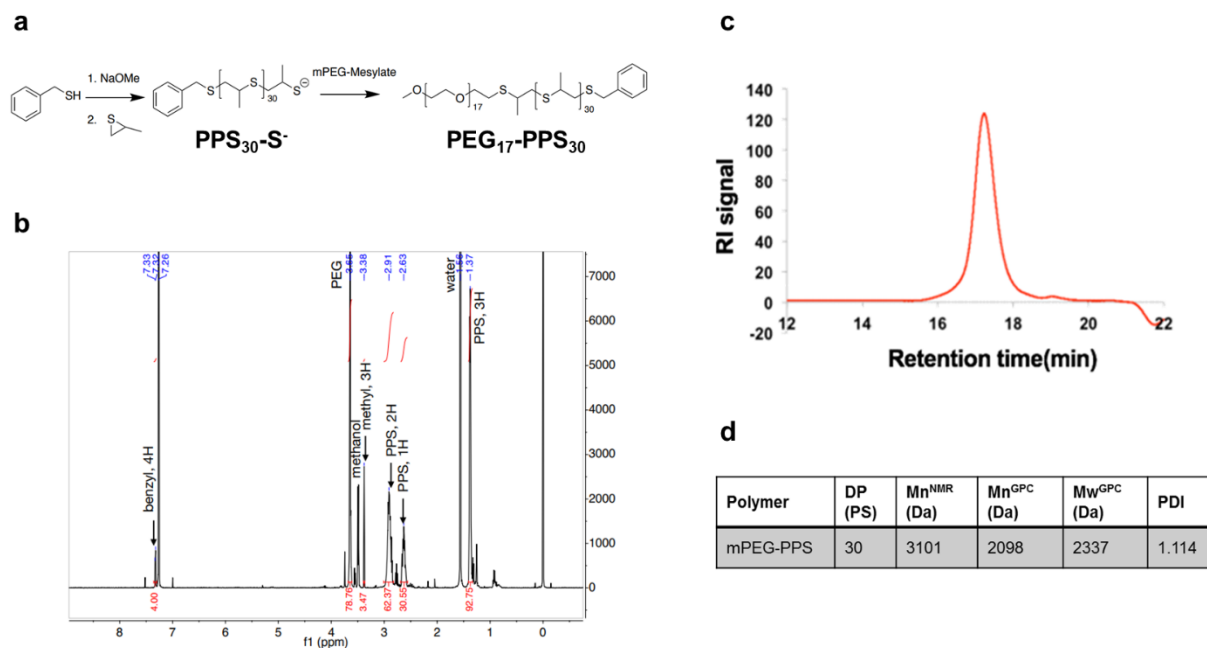


Figure S3 | Synthesis and characterization of PEG-PPS. **a**, Synthetic route, **b**, ¹H NMR spectrum, **c**, GPC trace, and **d**, summary of physicochemical properties of PEG-PPS.

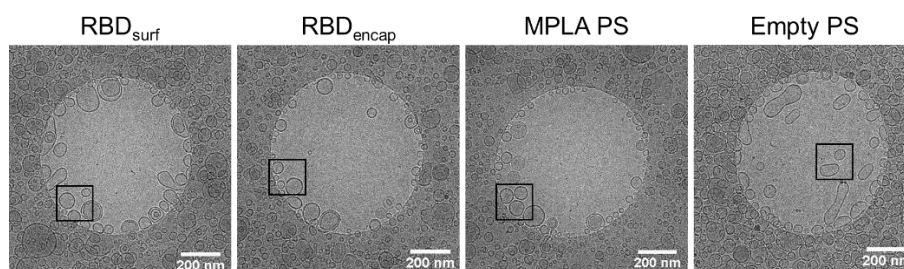


Figure S4 | Additional cryoEM images of PS. Black boxes indicate magnified region in Figure 1b.

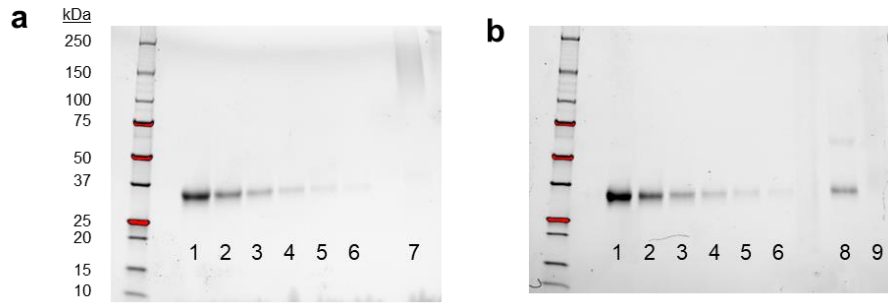


Figure S5 | PS stability by SDS PAGE after > 180 d at 4 °C. SDS PAGE of **a**, RBD_{surf} and **b**, RBD_{encap}. Lanes 1-6 represent RBD standard curve values of 400, 200, 100, 50, 25, and 12.5 $\mu\text{g mL}^{-1}$. Lane 7 (a) contains RBD_{surf} disrupted with Triton X. Lane 8 (b) contains RBD_{encap} disrupted with Triton X, and Lane 9 (b) contains undisrupted RBD_{encap}.

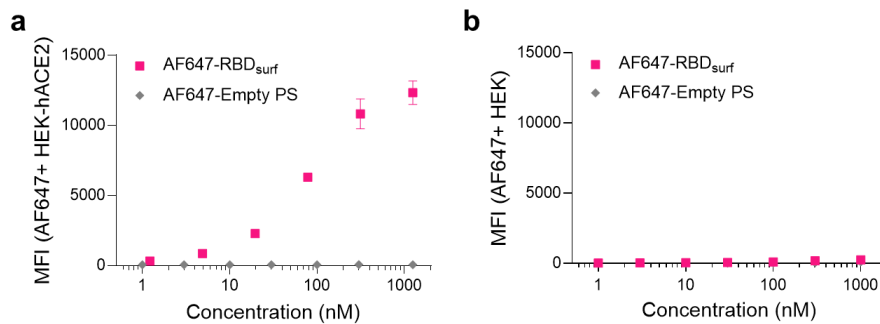


Figure S6 | RBD binding to HEK-hACE2 and HEK-293 cells. **a**, Mean fluorescence intensity (MFI) of AF647-labeled RBD_{surf} and empty PS bound to HEK-hACE2 cells characterized by flow cytometry. **b**, MFI of AF647-labeled RBD_{surf} and empty PS indicating an absence of binding to control HEK-293 cells. Data plotted as mean \pm SD for $n = 2$ replicates.

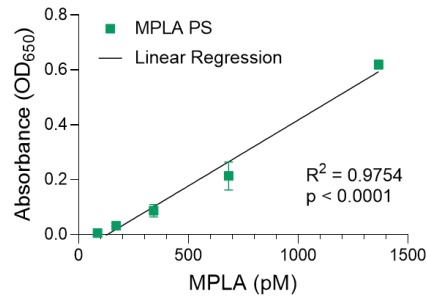


Figure S7 | MPLA PS as a TLR4 agonist. Linear concentration-dependent stimulation of HEK-Blue TLR4 reporter cells with MPLA PS. Data plotted as mean \pm SD for $n = 3$ replicates.

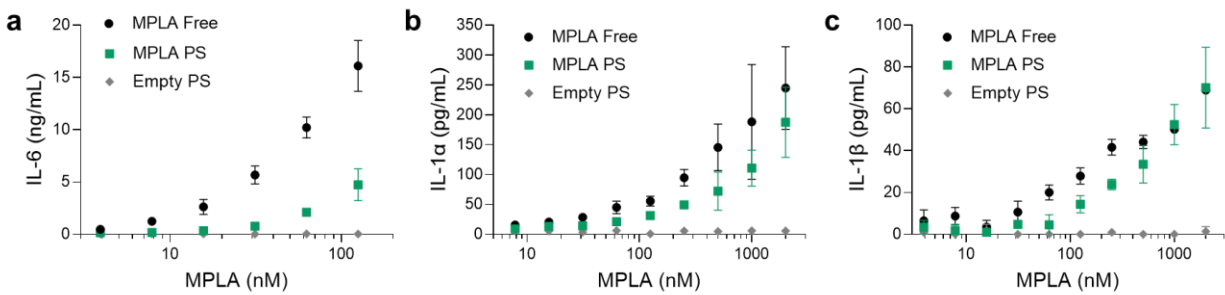


Figure S8 | *In vitro* activity of MPLA PS. Dose-dependent secretion of **a**, IL-6, **b**, IL-1 α , and **c**, IL-1 β from cultured murine bone marrow-derived dendritic cells stimulated by free MPLA, MPLA PS, or empty PS. Data plotted as mean \pm SD for $n = 3$ replicates.

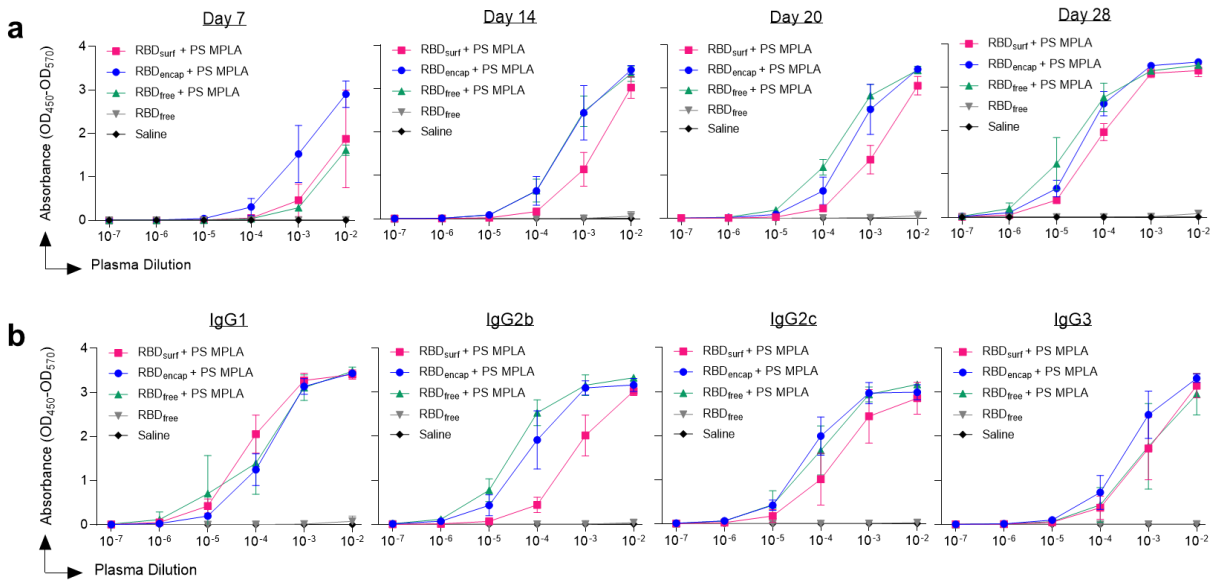


Figure S9 | ELISA absorbance vs dilution curves. Absorbance vs dilution for RBD-specific ELISAs for **a**, total IgG over time and **b**, IgG subtypes on day 28. Log-transformed curves were quantified by AUC in Figure 2. Data plotted as mean \pm SD and represent 1 of 2 experiments with $n = 5$ mice each.

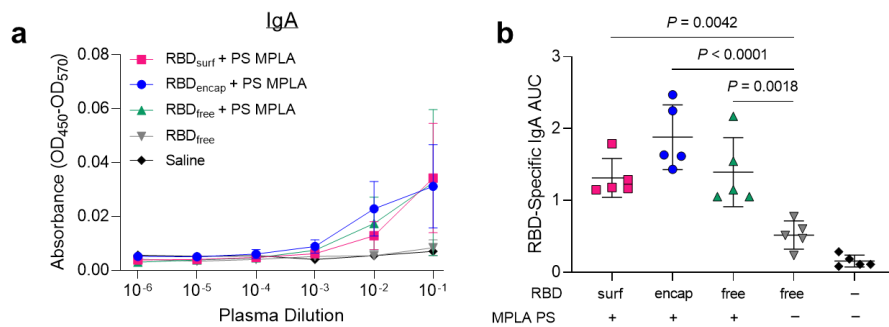


Figure S10 | Presence of IgA antibodies. **a**, Absorbance vs dilution for RBD-specific IgA ELISAs. **b**, Quantified AUC from (a). Symbols represent individual mice. Data plotted as mean \pm SD and represent 1 of 2 experiments with $n = 5$ mice each. Comparisons to unadjuvanted RBD_{free} were made using one-way ANOVA with Dunn's post-test.

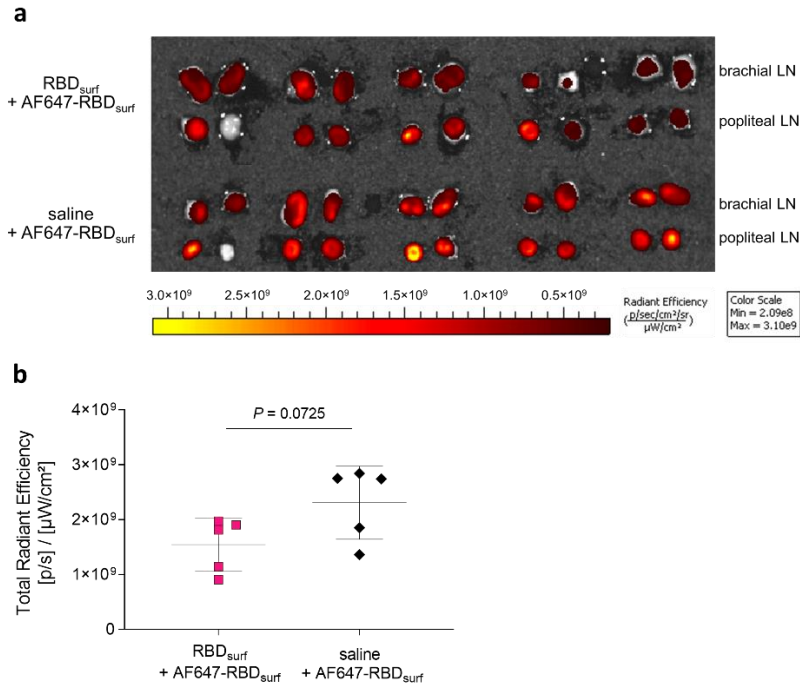


Figure S11 | Accumulation of RBD_{surf} in injection site draining lymph nodes. Mice pre-immunized with RBD_{surf} + MPLA PS or saline were injected with AF647-RBD_{surf}, and their lymph nodes were collected and imaged 24 h later. **a**, Whole-organ images of brachial and popliteal lymph nodes from mice pre-immunized with RBD_{surf} + MPLA PS (top) or saline (bottom). **b**, Background-subtracted quantification of (a) with symbols representing total radiant efficiency of all lymph nodes in an individual mouse. Comparisons were made using an unpaired, two-tailed t-test.

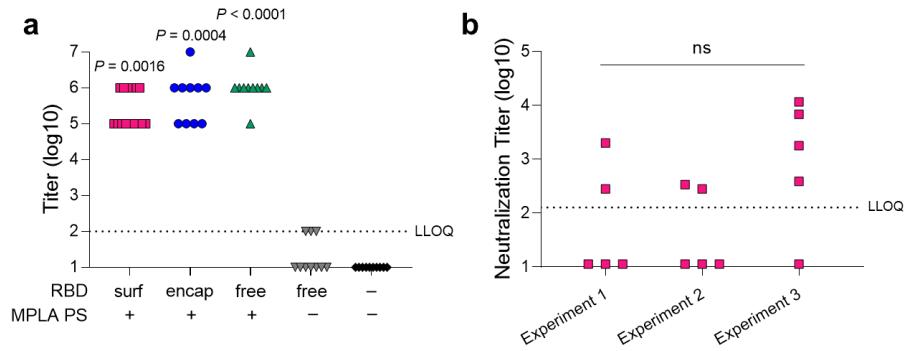


Figure S12 | IgG antibody and viral neutralization titers. **a**, Aggregate RBD-specific IgG antibody titers 1 week post-boost based on ELISA. Values below the LLOQ (= 2) are plotted as LLOQ/2. Titrers were determined as the $-\log$ of the lowest plasma dilution for which $(OD_{450} - OD_{570}) - (\text{average of blanks} + 4 \times \text{standard deviation of blanks}) > 0.01$. P values represent comparisons to unadjuvanted RBD_{free}. **b**, Virus neutralization titers for RBD_{surf} + MPLA PS across three different cohorts of $n = 5$ mice, indicating experiment reproducibility. Values below the LLOQ (= 2.11) are plotted as LLOQ/2.; ns $P = 0.11$. Symbols represent individual mice. Comparisons were made using a Kruskal-Wallis nonparametric test with Dunn's post-test.

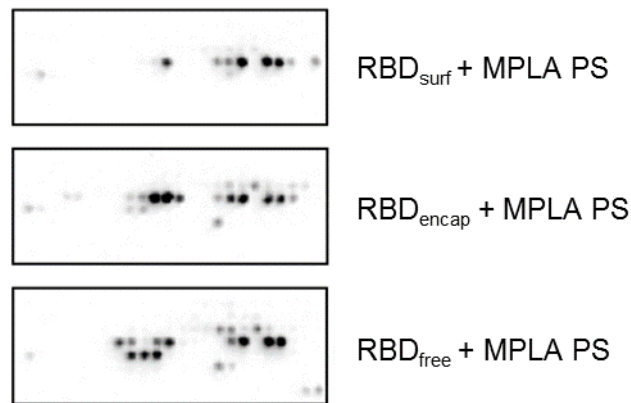


Figure S13 | Representative peptide array images. Boxes represent region of peptide array specific to the RBD of the Spike protein. Peptide arrays are quantified in Figure 3c.

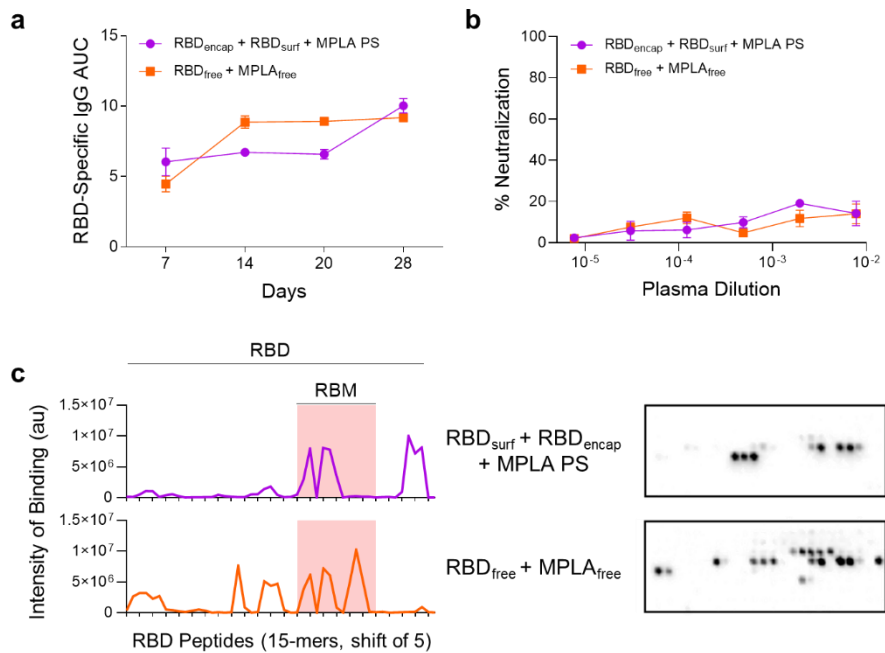


Figure S14 | Analysis of plasma by mice vaccinated with RBD_{surf} + RBD_{encap} + MPLA PS and RBD_{free} + MPLA_{free}. Mice received a priming dose on day 0 with a boost on day 21, and plasma was taken weekly to monitor production of RBD-specific antibodies. **a**, AUC of absorbance curve of RBD-specific IgG ELISAs for mice vaccinated with either 5 μ g RBD_{encap} + 5 μ g RBD_{surf} + MPLA PS or 10 μ g RBD_{free} + MPLA_{free}. Data plotted as mean \pm SD for n = 5 mice. **b**, Neutralization of SARS-CoV-2 infection of Vero E6 cells *in vitro*. Data plotted as mean \pm SEM for n = 5 mice. **c**, Epitope mapping using 15-amino-acid peptides with a 5-amino-acid shift, spanning the entire RBD sequence with representative images of peptide arrays.

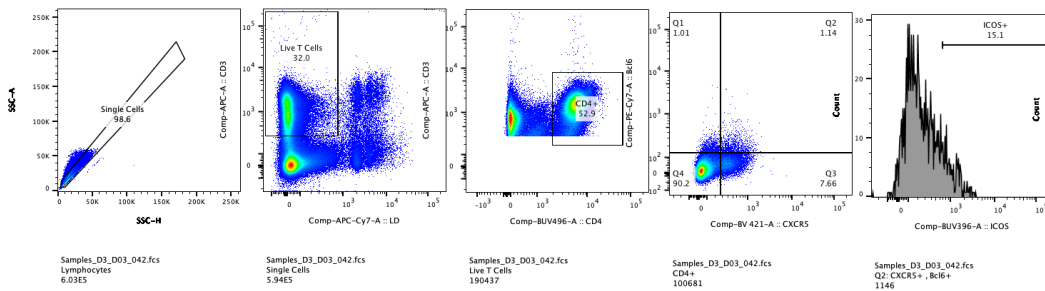


Figure S15 | Representative T follicular helper cell gating strategy.

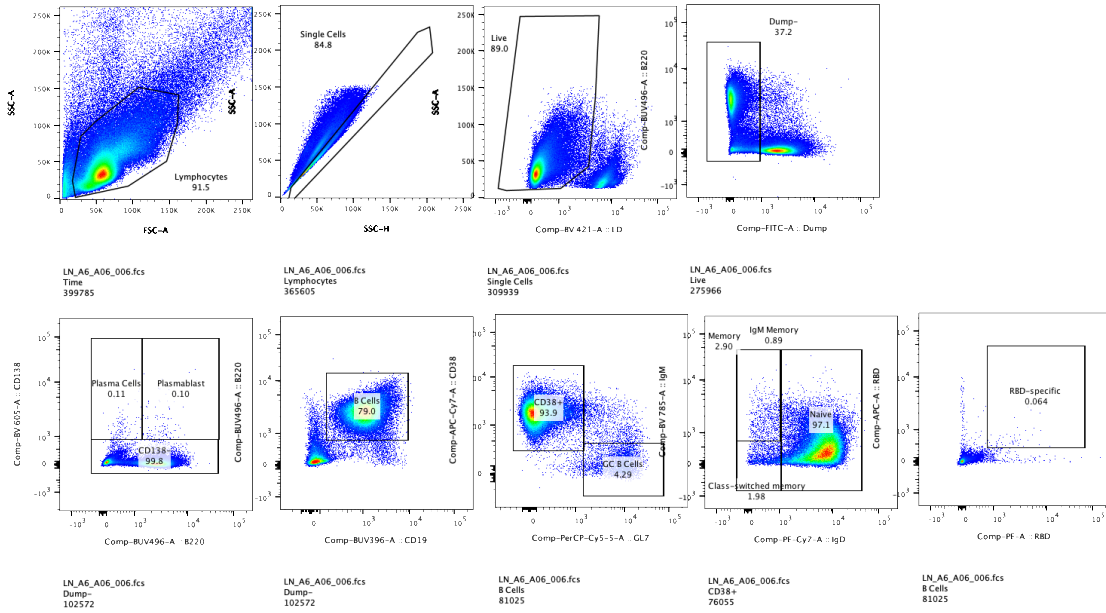


Figure S16 | Representative B cell gating strategy.

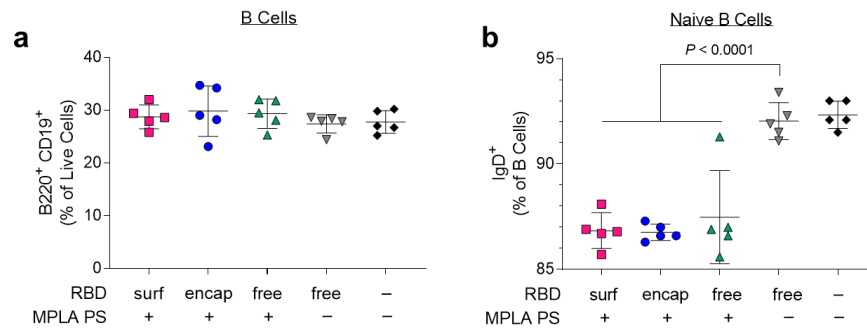


Figure S17 | Total and naïve B cells in vaccinated mice 1 week post-boost. a, Total B cells (B220⁺ CD19⁺) and **b**, naïve B cells (IgD⁺) in dLNs. Data plotted as mean \pm SD and represent 1 of 2 experiments with $n = 5$ mice each. Symbols represent individual mice. Comparisons to unadjuvanted RBD_{free} were made using one-way ANOVA with Dunn's post-test.

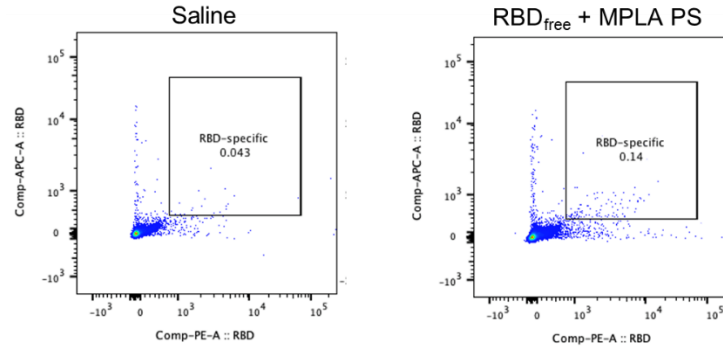


Figure S18 | Representative tetramer staining.

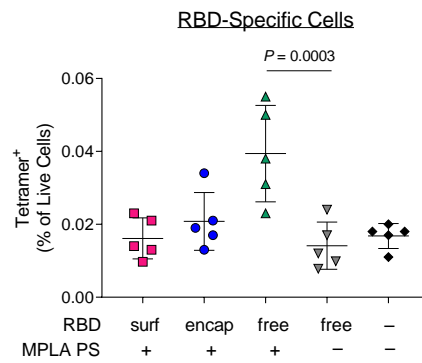


Figure S19 | RBD-specific cells in vaccinated mice 1 week post-boost. Tetramer⁺ cells in dLNs 1 week post-boost. Data plotted as mean \pm SD and represent 1 of 2 experiments with $n = 5$ mice each. Symbols represent individual mice. Comparisons to unadjuvanted RBD_{free} were made using one-way ANOVA with Dunn's post-test.

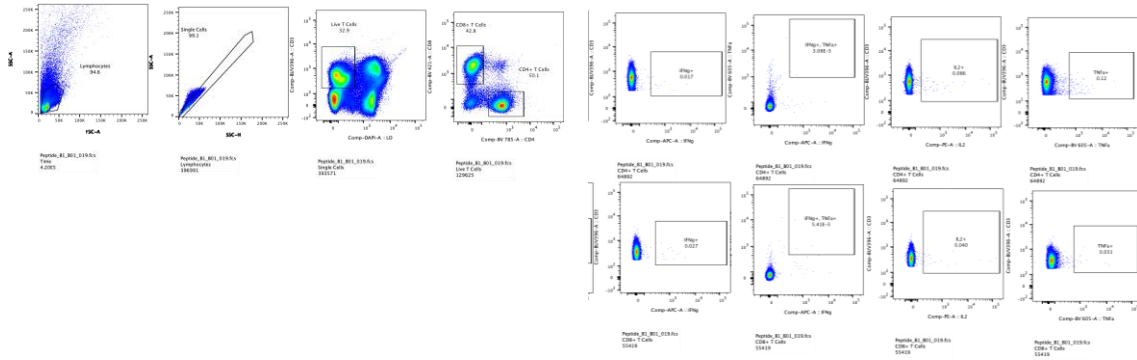


Figure S20 | Representative intracellular cytokine gating strategy.

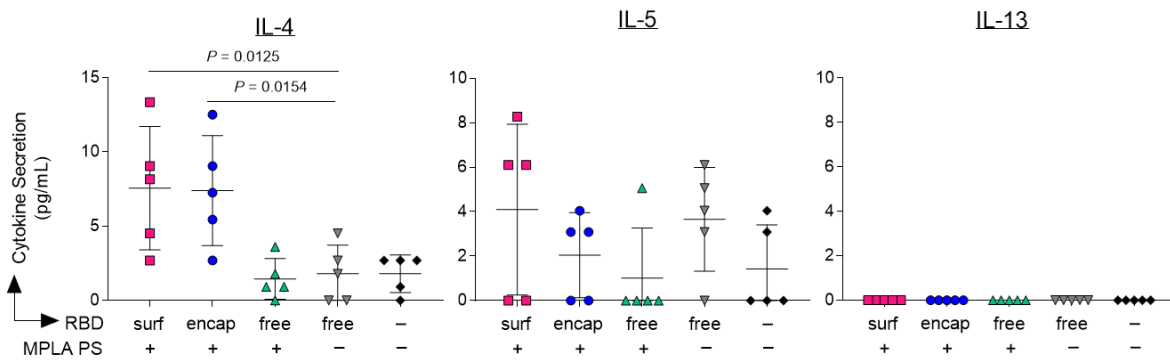


Figure S21 | Th2-type cytokines secreted upon *ex vivo* stimulation with RBD. Lymph node cells isolated from the dLNs of PS vaccinated mice 1 week post-boost were restimulated *ex vivo* with full RBD protein. After 3 d, levels of IL-4, IL-5, and IL-13 secreted into the supernatant were measured. Data plotted as mean \pm SD and represent 1 of 2 experiments with $n = 5$ mice each. Symbols represent individual mice. Comparisons to unadjuvanted RBD_{free} were made using one-way ANOVA with Dunn's post-test.

Table S1 | Summary of loading capacities of PS.

	Polymer (mg mL⁻¹)	Cargo (mg mL⁻¹)	Loading (wt%)
RBD _{surf}	7.96	0.127	1.57
RBD _{encap}	7.00	0.125	1.75
MPLA PS	3.49	0.241	6.46

Polymer concentration was determined by GPC, RBD concentration in RBD_{surf} was determined by CBQCA protein quantitation assay, RBD concentration in RBD_{encap} was determined by SDS PAGE, and MPLA concentration was determined by mass spectrometry.

Table S2 | Probes and antibodies for T_{fh} cell panel.

Marker	Color	Vendor
Viability Dye	eFluor 780	Invitrogen 65-0865-14
CD4	BV496	BD Horizon 612952
CD3	BUV737	BD Optibuild 741788
CD44	PerCpCy5.5	Invitrogen 45-0441-82
CXCR5	BV421	Biologend 145512
ICOS	BUV396	BD Horizon 565885
Bcl6	PE-Cy7	Biologend 358512

Table S3 | Probes and antibodies for RBD-specific B cell panel.

Marker	Color	Vendor
Viability Dye	Violet fluorescent reactive dye	Invitrogen L34964A
RBD-tetramer	PE	-
RBD-tetramer	APC	-
F4/80 (Dump)	FITC	Biologend 123107
CD11c (Dump)	FITC	Biologend 117306
Ly6c(Dump)	FITC	Invitrogen 53-5932-82
Ly6g (Dump)	FITC	Invitrogen 11-9668-82
CD4 (Dump)	FITC	Biologend 100406
CD8a (Dump)	FITC	Biologend 100706
B220	BUV496	BD Horizon 612950
CD19	BUV396	BD Horizon 565965
CD138	BV605	Biologend 142531
IgM	BV786	BD Optibuild 743328
IgD	PE-Cy7	Biologend 405720
CD38	APC-Cy7	Biologend 102727
GL7	PerCP-Cy5.5	Invitrogen 46-5902-82

Table S4 | Probes and antibodies for restimulation panel.

Marker	Color	Vendor
Viability Dye	eFluor 455 (UV)	Invitrogen 65-0868-14
CD3	BUV395	BD Horizon 563565
CD4	BV786	BD Horizon 563331
CD8	BV421	BD Horizon 563898
IFN λ	APC	Biolegend 505810
TNF α	BV605	Biolegend 506329
IL-2	PE	BD Pharmigen 554428

References

1. Amanat, F.; Stadlbauer, D.; Strohmeier, S.; Nguyen, T. H. O.; Chromikova, V.; McMahon, M.; Jiang, K.; Arunkumar, G. A.; Jurczynszak, D.; Polanco, J.; *et al.* A serological assay to detect SARS-CoV-2 seroconversion in humans. *Nat. Med.* **2020**, *26*, 1033–1036.
2. Scott, E. A.; Stano, A.; Gillard, M.; Maio-Liu, A. C.; Swartz, M. A.; Hubbell, J. A. Dendritic cell activation and T cell priming with adjuvant- and antigen-loaded oxidation-sensitive polymersomes. *Biomaterials* **2012**, *33*, 6211–6219.
3. Xiong, X.; Qu, K.; Ciazynska, K. A.; Hosmillo, M.; Carter, A. P.; Ebrahimi, S.; Ke, Z.; Scheres, S. H. W.; Bergamaschi, L.; Grice, G. L.; *et al.* A thermostable, closed SARS-CoV-2 spike protein trimer. *Nat. Struct. Mol. Biol.* **2020**, *27*, 934–941.
4. Klein, S.; Cortese, M.; Winter, S. L.; Wachsmuth-Melm, M.; Neufeldt, C. J.; Cerikan, B.; Stanifer, M. L.; Boulant, S.; Bartenschlager, R.; Chlanda, P. SARS-CoV-2 structure and replication characterized by in situ cryo-electron tomography. *Nat. Commun.* **2020**, *11*, 5885.
5. Ke, Z.; Oton, J.; Qu, K.; Cortese, M.; Zila, V.; McKeane, L.; Nakane, T.; Zivanov, J.; Neufeldt, C. J.; Cerikan, B.; *et al.* Structures and distributions of SARS-CoV-2 spike proteins on intact virions. *Nature*, **2020**, *288*, 498–502.
6. Han, J.; Zhu, Z.; Qian, H.; Wohl, A. R.; Beaman, C. J.; Hoyer, T. R.; Macosko, C. W. A simple confined impingement jets mixer for flash nanoprecipitation. *J. Pharm. Sci.* **2012**, *101*, 4018–4023.
7. Allen, S.; Osorio, O.; Liu, Y-G.; Scott, E. Facile assembly and loading of theranostic polymersomes via multi-impingement flash nanoprecipitation. *J. Control. Release* **2017**, *262*, 91–103.
8. Hamdy, S.; Haddadi, A.; Somayaji, V.; Ruan, D.; Samuel, J. Pharmaceutical analysis of synthetic lipid A-based vaccine adjuvants in poly (d,l-lactic-co-glycolic acid) nanoparticle formulations. *J. Pharm. Biomed. Anal.* **2007**, *44*, 914–923.
9. Lutz, M. B.; Kukutsch, N.; Ogilvie, A. L. J.; Röβner, S.; Koch, F.; Romani, N.; Schuler, G. An advanced culture method for generating large quantities of highly pure dendritic cells from mouse bone marrow. *J. Immunol. Methods* **1999**, *223*, 77–92.